



HAL
open science

High resolution characteristics of turbulence tied of a fish farm structure in a tidal environment

Emmanuel Poizot, Yann Méar, Sylvain Guillou, Eric Bibeau

► **To cite this version:**

Emmanuel Poizot, Yann Méar, Sylvain Guillou, Eric Bibeau. High resolution characteristics of turbulence tied of a fish farm structure in a tidal environment. Applied Ocean Research, 2021, 108, pp.102541. 10.1016/j.apor.2021.102541 . hal-03722576

HAL Id: hal-03722576

<https://cnam.hal.science/hal-03722576>

Submitted on 22 Mar 2023

HAL is a multi-disciplinary open access archive for the deposit and dissemination of scientific research documents, whether they are published or not. The documents may come from teaching and research institutions in France or abroad, or from public or private research centers.

L'archive ouverte pluridisciplinaire **HAL**, est destinée au dépôt et à la diffusion de documents scientifiques de niveau recherche, publiés ou non, émanant des établissements d'enseignement et de recherche français ou étrangers, des laboratoires publics ou privés.

Copyright

High resolution characteristics of turbulence tied of a fish farm structure in a tidal environment

Emmanuel Poizot^{a,b,*}, Yann Méar^{a,b}, Sylvain Guillou^b, Eric Bibeau^c

^a*LUSAC-Intechmer, Conservatoire National des Arts et Métiers B.P. 324, 50103 Cherbourg En Cotentin, France*

^b*Normandy University, UNICAEN, LUSAC, 60 rue Max Pol Fouchet, 50130 Cherbourg En Cotentin, France*

^c*University of Manitoba, Mechanical and Manufacturing Engineering Department, Winnipeg, Canada*

Abstract

Characterization of tidal flow variations and turbulence levels surrounding aquaculture infrastructures contribute to optimal fish production management and to a good environmental quality assessment. Such flow characterization was performed in Cherbourg Roadstead, France. An acoustic Doppler current profiler was used to measure flow velocities and a vertical microstructure profiler to assess turbulence levels and length scales in the vicinity of a commercial fish farm. Flow measurement results show that fish nets increase local turbulence level, impacting the flow and vorticity produced by the nets, contributing to more scouring of the ocean floor. A wavelet analysis allows to evaluate vortex sizes and where they are localized along the water column. Flow characterization shows these vortices are produced in the vicinity of fish nets and in their wake. Larger and more energetic turbulent structures are produced below aquaculture cages, which extend into the wake and onto the ocean floor.

Keywords: tide currents; fishnets; vorticity; wavelet; aquaculture

1. INTRODUCTION

Fish farming started in the seventies. Aquaculture is poised to take an increasingly significant part as a food source (Duarte et al., 2009; Holmer, 2010; Food and Organization, 2020). The growing number of farms has consequences on the marine environment and on the use of natural resources.

*Corresponding author

Email address: emmanuel.poizot@lecnam.net (Emmanuel Poizot)

Increasing environmental control is required to preserve environmental quality and to enhance product quality.

These controls are necessary due to the ecological disturbance of the breeding site linked, in particular, to metabolic discharges from fishes. Faeces are particularly rich in nitrogen, ammonia, phosphorus, trace metals and organic carbon. These faeces can be released in particulate or dissolved form. The accumulation of these wastes can lead to anoxic conditions that affect fish welfare and growth (Thetmeyer et al., 1999). Their dispersion can also affect the farm environment both locally and on a more global scale (Skogen et al., 2009).

With the aim of improving the quality of the environment and consequently the health of the farm, many studies have been carried out (Klebert and Su, 2020) to reduce the impact of production structures and, if necessary, promote the dilution of waste.

Since the work of Gowen et al. (1989) who pioneered the application of numerical models to study local cage-environment interactions and the dispersion of effluents in the environment, much work has been carried out. At the local scale, Masaló et al. (2008); Gjøvsund and Enerhaug (2010); Gorle et al. (2019) studied the hydrodynamic performance of the different cage models and their behavior. The action of the flow current on the cages (Lader et al., 2008; Gansel et al., 2018) has been addressed because of the deformations of these cages limiting the space dedicated to fish and modifying their hydrodynamic behavior. In the same theme, Bi et al. (2014) studied the action of waves while considering biofouling of the nets.

Recently, Xu et al. (2015) showed that vertical mixing plays a key role in the hydrodynamic environments of the sea-cage farms. Eddies can be generated in the wake or in different part of the cages. The turbulence appears to be a key parameter for the understanding of the cages-hydrodynamic interaction (Gansel et al., 2018).

Since Panchang et al. (1997), the numerical approach to model the impact of farming at greater distances has also been the subject of several works. Cromey et al. (2002) proposed one of the first numerical tools concerning the modeling and biological effects of solid waste deposit. Used worldwide, this tool subsequently evolved (Chamberlain et al., 2006; Chamberlain and Stucchi, 2007). Computational Fluid Dynamic (CFD) to study flow perturbations in and around gravity cages is largely used (Patursson, 2008; Patursson et al., 2010; Zhao et al., 2013; Bi et al., 2014; Cornejo et al., 2014). Performed on scaled cages, most of these CFD simulations results had been verified with experimental measurements in flumes and tow tanks. Recently, Winthereig-Rasmussen et al. (2016) performed a CFD simulation of the flow through a full-scale commercial salmon farm and compared the results with field mea-

surements made at the same farm (Klebert et al., 2015; Johansson et al., 2014). Discrepancies between simulated and measured data were due to an increased net solidity from cages deformed by the flow and a block effect from the fish inside the cage. Poizot et al. (2016) showed that in spite of favourable environmental conditions (sea protection and tide currents which regularly refresh the water), periods of non-negligible fish mortalities can be observed to occur without clear evidence of their origin. They showed through turbidity measurements and numerical modelisation, that in some cases the flow acceleration under the cages can be at the origin of sediment re-suspensions and bio-deposits. As a consequence, particles which enter the fishnet can have different origins: external source, sea-bottom, or nets themselves. They observed that turbulent dispersion is a key ingredient for such a behaviour, as it can lead particles towards a large recirculation cell behind the net and force particle faeces, uneaten food and more generally other wastes, from the bottom to be lifted up and reach the rear of the net. They observed that the numerous vortices downstream from the cages are responsible for complex transfers of re-suspended particles from the sea bottom to the sea surface. Therefore, high turbidities due to a self-contamination process in the vicinity of the cages can exist under the sole effect of the turbulence tied up to high velocities below the fishnets and are likely to happen even in the absence of external sources of pollution in the upstream flow.

One of the main conclusions of the various works aiming to numerically model the transport of effluents linked to aquaculture in the marine environment is that the variability of water flows on the various temporal and spatial scales and their action on flexible cages leads to complex interactions (Klebert et al., 2015; Gansel et al., 2018; Poizot et al., 2016). In order to be able to model more precisely the dynamics of the structure of the water column and the dispersion of effluents from breeding cages, it appeared necessary that the numerical models have an accurate representation of transfers due to turbulent diffusion. To test turbulence closure patterns with field data, measurements of the turbulence parameters can now be made in the field (Winthereig-Rasmussen et al., 2016).

Acoustic Doppler current profilers (ADCP) allow to obtain partial information on the turbulence of the water flow (Guerra and Thomson, 2017; Lu and Lueck, 1999; Stacey et al., 1999). Their relatively low sampling frequency, up to 16 Hz, only allows to capture turbulent structures whose size is pluri-decimetric. It was only recently (Klebert and Su, 2020) that a free-fall profiler was implemented to measure the micro-scale turbulence near cages from sea surface to the bottom. Vertical micro-structure profilers (VMPs) are high resolution instruments specifically developed to produce *in-situ* measurements of turbulence characteristics (Lu and Lueck, 1999). It allows to

measure vortices from ~ 0.003 m to 1 m, over the water column (McMillan et al., 2015).

A VMP is used to give precise and accurate measurements of turbulent characteristics around a fish farm production site in this study. It should be used to reproduce the detailed flow inside a fish farm by CFD modelling.

The fish farm is introduced in Section 2. Materials and processing are introduced in Section 3, in particular, this section contains a review of VMP's technology and measurement principles. Results and discussions are presented in Section 4 before the conclusion in Section 5.

2. FISH FARM

Measurements were conducted in the Cherbourg roadstead, Normandy, France, the European's largest artificial roadstead. It has an area of $\sim 1,500$ ha, divided into the "Grande rade" and the "Petite rade", as shown in Fig.1. The "Grande rade" (1,300 ha) is in contact with the open sea through "West gate", "East gate" and "Collignon gate". The roadstead is under the influence of a semi-diurnal tide, giving an oscillating volume of $\sim 80,000$ m³ during spring tide and a tidal amplitude of ~ 6 m (Merceron et al., 2002). The maximum depth is 25 m with a mean depth of ~ 15 m. The mean water temperature is below 8-9°C in winter and reaches 17-18°C at the end of the summer.

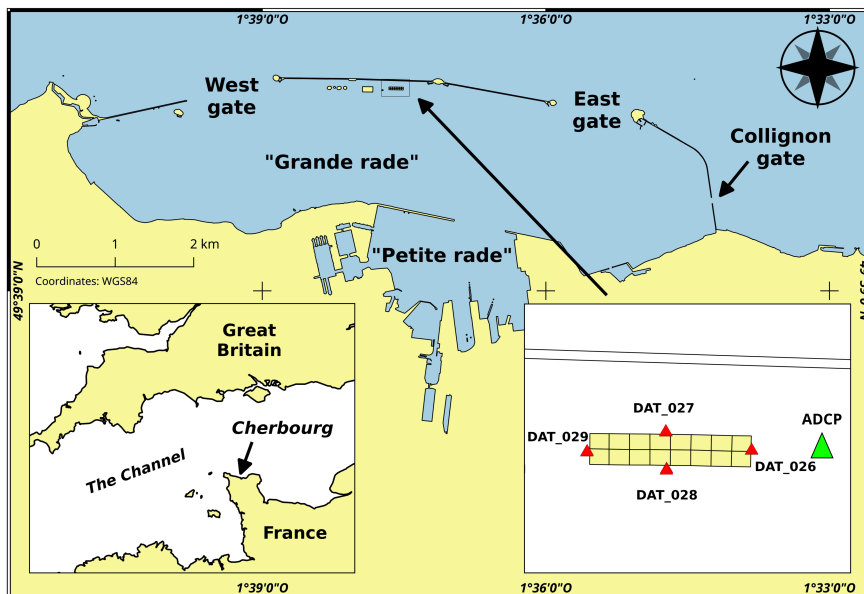


Figure 1: The Cherbourg roadstead (France). Red triangles represent the locations where VMP profiles were realized around fishnet structures of the aquaculture farm. Green triangle is the location where the ADCP was moored.



Figure 2: View of the aerial parts of fishnet structures of the salmon fish farm located in the Cherbourg roadstead (from <https://www.keldelice.com/producteurs/saumon-de-france>).

The Cherbourg roadstead is characterized by a particular tidal hydrodynamic. The predominant current is eastward during the flood and westward

during the ebb. The flood stream enters through the West gate and stand out mainly through the East gate and to a lesser extent, through the Collignon gate. This is the opposite to ebb. During the flood, depending on the interactions between the bathymetry, the coastline and tidal currents, gyres may form locally with counter-clockwise rotation (Merceron and Gaffet, 1994). This is the case at the south edge of the central dike (Fig.1). In the fish farm site, tidal currents are asymmetric: the flood currents are oriented eastward 30% of the time and ebb currents are oriented westward 70% of the time (Merceron and Gaffet, 1994).

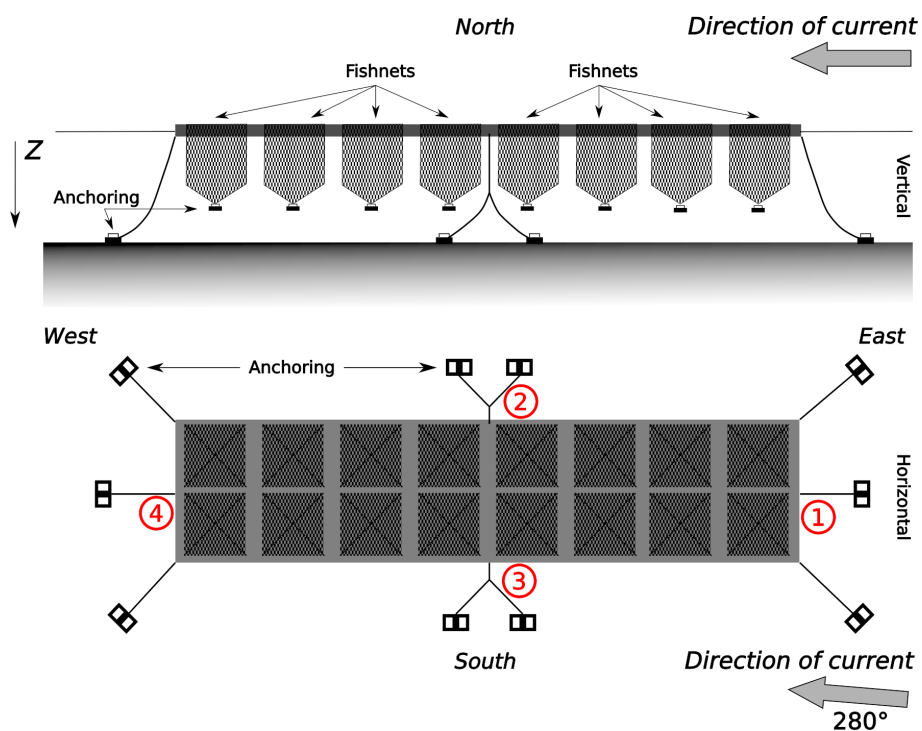


Figure 3: Vertical (up) and horizontal (down) details of the rectangular fishnet structures around which measurements were performed. The direction of the current during the measurement period is indicated on both vertical and horizontal view. The four cardinal directions show general orientation of the nets. Red numbers surrounding with a red circles are respectively locations of DAT_026, DAT_027, DAT_028 and DAT_029 measurements stations.

The aquaculture farm has been operational since 1990. It is located 50 m south the central dike (Fig.1) and covers an area of ~ 15 ha (1.5 km long and 100 m wide). Nowadays, around 1,000 tons of salmonids (*Salmo salar*) are produced per year. The mean water depth below the farm ranges from 11 m to 13 m from the zero tidal level. The production structures are composed

of a mix of cylindrical (\varnothing 40 m) and cubic nets (40 m x 160 m) as shown in Fig.2 and Fig.3. The average bottom of the nets lies between 7 to 8 m below the sea surface. ADCP and VMP measurements took place around a structure containing eighteen square nets (2 x 8). The nets were made with synthetic ropes organized in square meshes of size 2 x 2 cm. The mean density of fish in each net was around 12 kg.m^{-3} . As the nets are regularly cleaned, biofouling is minimum. A few small algae ($< 1 \text{ cm}$) form on the net ropes.

3. MATERIALS AND METHODS

3.1. Vertical Microstructure Profiler (VMP)

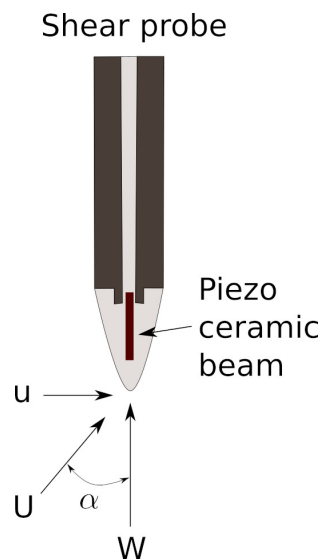


Figure 4: Shear stress probe located on VMP 250 (Rockland Scientific). W is fall rate of the profiler, u is the horizontal component of the turbulence velocity, U is the total velocity and α is the AOA.

The VMP has two shear probes (Fig.4) and two thermistors. VMPs are mainly shaped as cylinders with sensors located at one end (Fig.4). Generally, measurements are taken with the instrument falling freely vertically along the water column, with sensors first. The VMP is shaped so as to fall vertically at a constant velocity. To do so, it is equipped with a drag brush which control the falling velocity of 0.8 m.s^{-1} . According to the VMP model employed, the drag brush is specific to the instrument so that the drag forces are taken into account. The probe moves axially through the water at a speed W high enough to apply Taylor's frozen turbulence hypothesis (Taylor, 1938; Moin,

2009). The horizontal component of the turbulent velocity, u , turns the total velocity, U , into the vectorial sum of W and u , *i.e.* $\vec{U} = \vec{W} + \vec{u}$. It induces an angle of attack (AOA), called α (Fig.4). The AOA induces a lift force over the surface of the probe which bends the piezo-ceramic of the probe. The bending of the probe is converted into an electrical signal ($e = SWu$, with S as the sensitivity of the probe). This electrical signal is sampled at 1 kHz with a sign function of the direction of the bending. Under the hypothesis of Taylor "frozen field", the time rate-of-change of u is converted into a spatial gradient, to yield the vertical shear of horizontal velocity, according to:

$$\frac{\partial u}{\partial z} = \frac{E}{W^2 S} \quad (1)$$

The shear probe is only sensitive to a single component of velocity—the component oriented at right angles to the probes' axis and oriented normal to the wide surface of the piezo beam. Two shear probes are used, one of which is rotated by 90° around its axis. This gives two shear components, $\partial u/\partial z$ and $\partial v/\partial z$. As sensors are very sensitive, instrumental noise and disturbance of the main body need to be removed from the shear signals (Macoun and Lueck, 2004).

In the present work, a VMP-250 model from Rockland Scientific (Lueck et al., 2013) allowed eddies measurements in the range ~ 0.003 m to 1 m. The length of the probe acts as a low pass filter, vortex with size greater than the length of the probe cannot be measured. Two temperature sensors (thermistors) are also present on that model. They measure temperature fluctuations along the water column and their signal is sampled at the same frequency as the shear probes.

Several VMP profiles were carried out at each station around the immersed structure. One profile is studied per station according the following criteria:

- the probe velocity, W , should be fairly constant,
- body vibrations must have a low impact on the shear signals,
- the VMP roll angle must be within an acceptable range (less than $\pm 5^\circ$).

3.2. Acoustic Doppler Current Profiler (ADCP)

In order to quantify the tidal current characteristics, an acoustic Doppler current profiler (ADCP) was moored from the 4th to the 9th of April 2015. It was placed at the eastern part of the fish farm (Fig.1). The instrument used was a Teledyne RDI Workhorse Sentinel with a frequency of 600 kHz. During

the VMP survey, the measurements of the flow characteristics were made at a frequency of 1 Hz and averaged over 5 minutes to obtain the mean flow velocities and directions. The ADCP was set to sample the water column along 13 cells of 1 m height each (Fig.5).

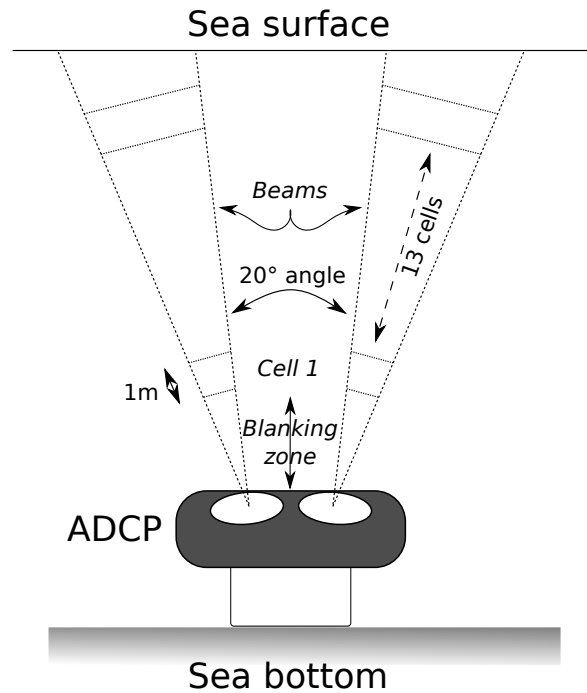


Figure 5: ADCP physical deployment settings during the period of measurements. Only two from the four beams are represented.

Directly above the device's head, no measurement can be made, due to technical limitations. This area is called the blanking zone. In the present study, this zone is about 1 m and the ADCP's transducers are at 0.7 m above the sea bottom, so that the first cell of measurements starts at 1.7 m above the sea bottom.

3.3. Data treatments

Classical treatments of the VMP data sets are made through Matlab scripts (Lueck, 2013) provided by Rockland Scientific. These scripts allow in a first time to apply a set of corrections and filtering on the raw data to obtain different graphs to assess data validity. Then, fast Fourier transform (FFT) based analysis are computed to highlight turbulence characteristics. The FFT analysis can be performed under the assumption that the signal

is stationary (Massel, 2001). If that's not the case, the use of FFT is not relevant (del Alamo and Jimenez, 2009).

In order to enhance the study of VMP shear signals, a wavelet analysis was conducted. Wavelet analysis is considered superior to Fourier analysis because it unfolds a time series in both frequency and time domains (Torrence and Compo, 1998), it requires no assumption of stationary, and can determine not only the dominant modes of variability in frequency but also how those modes vary over time (Torrence and Compo, 1998; Tseng et al., 2012). Wavelet analysis of a time series is essentially the systematic application of a set of band-pass filters whose bandwidths are proportional to the central periods (Torrence and Compo, 1998; Mallat, 1989). Wavelet analysis is able, at a minimum, to give the same information as FFT, but with less constraints of application. The main interest of wavelets is that they localize frequencies over time. This last information is essential in the case of 3D CFD models which needs not only to simulate the right range of turbulent frequencies, but also the same location in the modeled domain.

Wavelet computation was realized using R Language (R Core Team, 2016), through the use of the "WaveletComp" library (Roesch and Schmidbauer, 2014).

4. RESULTS AND DISCUSSIONS

As the flow direction was 280° during VMP surveys (Fig.6), DAT_026 station is at the inlet of the studied domain and DAT_029 at the outlet, *i.e.* in the wake of the fishnet. The two other stations, DAT_027 and DAT_028 are located respectively North and South were the water flows on the longest sides of the structures (Fig.1 and 3).

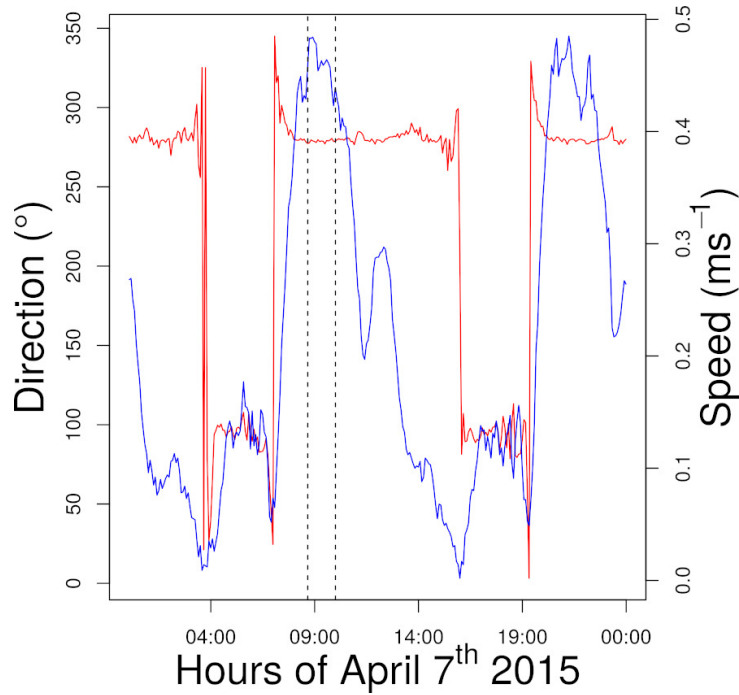
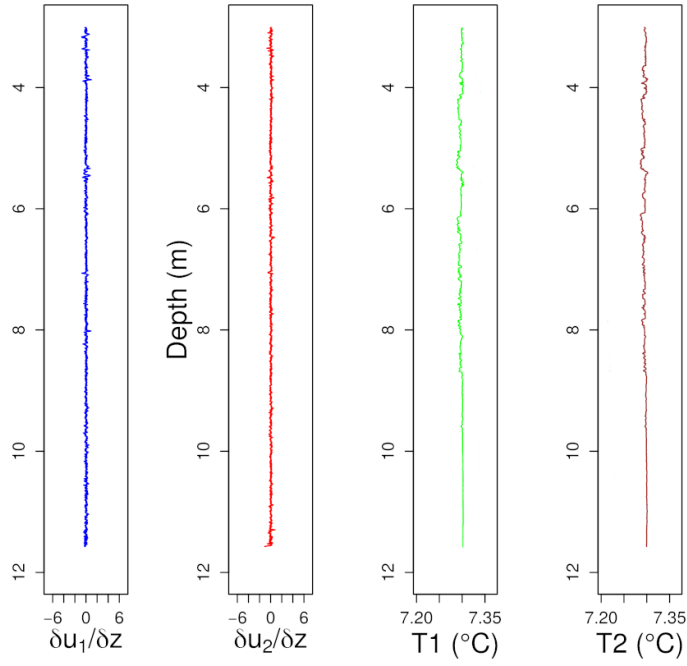


Figure 6: Mean direction (red) and speed (blue) of current at the fish farm (Fig.1) the 7th of April 2015. Dashed lines represent the start and end of the time period of the VMP measurements.

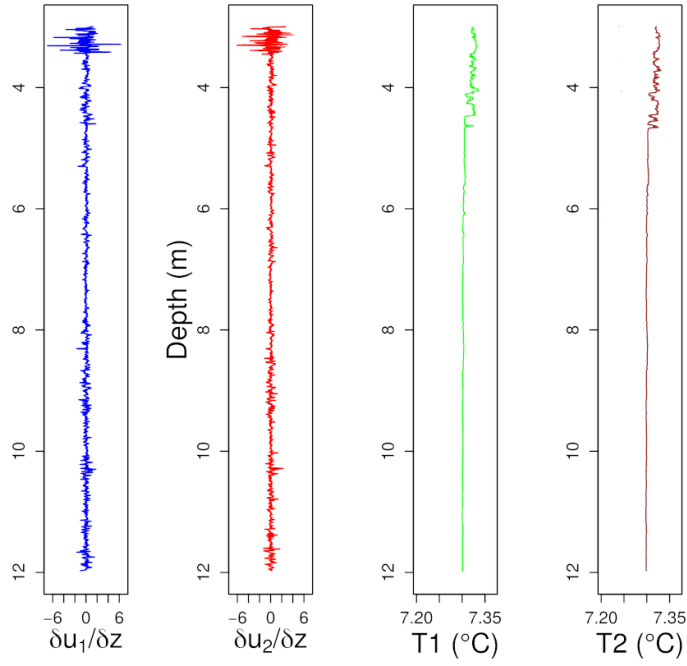
VMP measurements were performed the 7th of April 2015. The measurement period was chosen to correspond to the maximum flow velocity of the tidal cycle (Fig.6). Under these environmental conditions, the hydrodynamic constraints are at their maximum between currents and fish farm structures, so that the turbulence generation is expecting to be also at its maximum, allowing better highlighting fish farm structure impacts on flow characteristics. The two thin dashed lines on Fig.6 represent the start and the end time period of the survey, *i.e.* 90 min.

At the ADCP location, the water flows westward during ebb in the direction 270°–280°, 2/3 of the time. It flows eastward during flood in the direction 90°–100°, 1/3 of the time. Flow velocities during the ebb are not constant and range from 0.20 to 0.50 m.s⁻¹. The maximum speed is reached during the first half of the ebb current period, and ongoing fallout until the current changes back to flood. During flood, flow velocities are globally more constant but three or four times lower, ranging from 0.10 to 0.15 m.s⁻¹. During the VMP measurement time, the mean water velocity was 0.45 m.s⁻¹ and the mean direction was 280° (Fig.3).

Figures 7 and 8 show intensity variations of VMP shear probes Sh_1 and Sh_2 , and of the temperature gradient measured by the thermistors, *i.e.* T_1 and T_2 at stations DAT_026-027 and stations DAT_028-029, respectively for the four chosen profiles. Intensity of the signal variations of the shears is a high frequency indication of the level of turbulence on the water column. Temperature gradient variations are low frequency qualitative information of turbulence characteristics modifications. It can be used to suspect presence of vortices with size greater than 1 m.

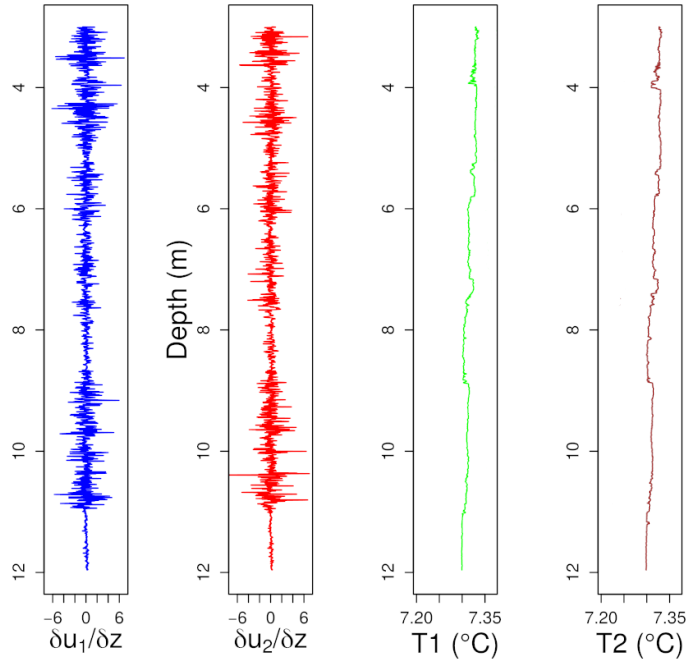


(a) Profile DAT_026

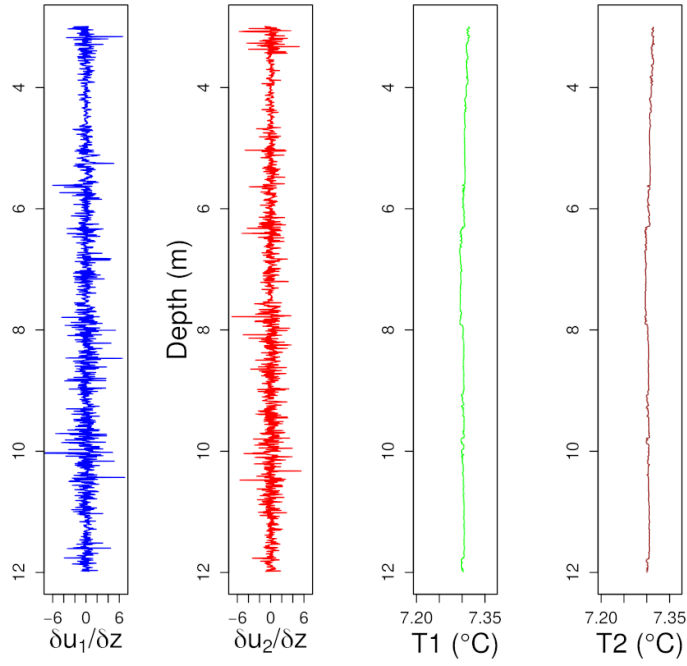


(b) Profile DAT_027

Figure 7: Raw data for each profile at stations DAT_026 and DAT_027, with $\delta u_1/\delta z$ for Sh_1 and $\delta u_2/\delta z$ for Sh_2 . T1 and T2 correspond to the two thermistors.



(a) Profile DAT_028



(b) Profile DAT_029

Figure 8: Raw data for each profile at stations DAT_028 and DAT_029, with $\delta u_1/\delta z$ for Sh_1 and $\delta u_2/\delta z$ for Sh_2 . T1 and T2 correspond to the two thermistors.

Figures 7 and 8 allow to classify the different profiles in terms of intensity variations of shears. DAT_026 profile is the less energetic one, since few variations are present both on shears and temperatures. The profile DAT_027 has some more variations on its signals. Near the sea surface at 3.5 m strong fluctuations are present. Until 8 m, they decrease slightly. From this depth to the end of the profile, fluctuations are constant but more pronounced. In terms of intensity variations on shears and temperatures, various energetic domains are highlighted for DAT_028 station. A first domain is recognized with high fluctuations until 4 m depth. A succession of highly characterized episodes of high and low energy followed one another until 11 m. Below this latter depth, energetic level is low. At DAT_029 station, after a level of high fluctuations until 3.5 m, the energy falls abruptly. From this depth, both Sh_1 and Sh_2 highlight growing intensity variations to the end of the profile.

Figures 9 and 10 show the wave number spectra of the shears at the four stations. These graphics allow to highlight main vortices structures present on the water column. Abscissa corresponds to wave number, k , in count per metre (cpm) and the ordinate is the dissipation rate, $\Phi_{(k)}$ ($s^{-2} \cdot \text{cpm}^{-1}$). The thin black lines correspond to the fit of the Nasmyth model (Lueck, 2015; Nasmyth, 1970) for dissipation rates defined on $\partial u_1 / \partial z_{clean}$ (*i.e.*, Sh_1) clean and $\partial u_2 / \partial z_{clean}$ (*i.e.*, Sh_2) clean (*i.e.*, filtered) signals (Oakey, 1982) respectively. The ϵ value used to compute the Nasmyth model is indicated in the graphic legend. Wave numbers are considering as significant when 1) the signal is higher to its corresponding Nasmyth curve, and 2) the signal is located between the lowest value of wave number and the integration limit, marked by a blue and red triangle for respectively $\partial u_1 / \partial z_{clean}$ and $\partial u_2 / \partial z_{clean}$. These graphics are computed through a Fourier transform of the original signal.

DAT_026 inlet station shows the less energetic spectrum ($\epsilon \approx 10^{-4} W \cdot kg^{-1}$) which confirms previous observations on Fig.7. This low energetic level makes detection of particular frequency/size difficult. This is in particular the case for the highest frequencies, *i.e.* small size vortex ($1/k$). Sh_1 signal highlights three main peaks (0.035 m, 0.040 m), 0.058 m and 0.18 m, whereas Sh_2 shows two sizes, 0.52 and 0.13 m. These characteristics are in agreement with the two different Nasmyth fitted models which are shifted, indicating an anisotropy of the two signals Sh_1 and Sh_2 .

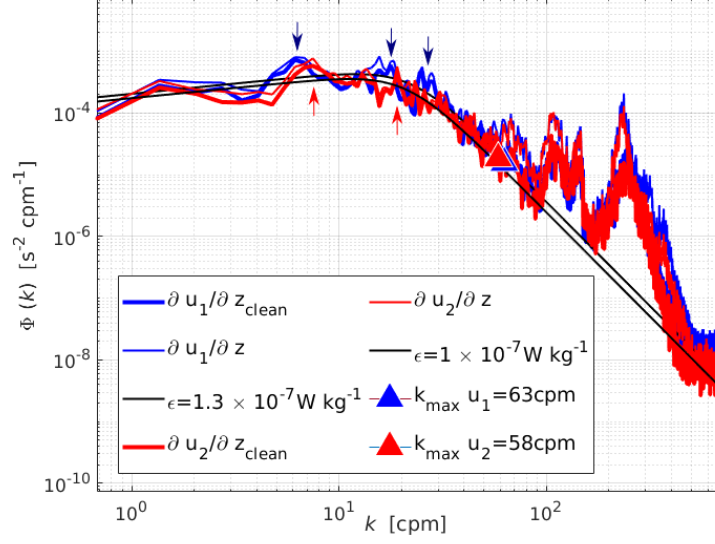
The three other stations are more energetic in the range $\epsilon \approx 10^{-3} W \cdot kg^{-1}$ to $\epsilon \approx 10^{-2} W \cdot kg^{-1}$, that is 10 to 100 times more than DAT_026 station.

DAT_027 is also characterized by an anisotropy of the signals, but more important than at DAT_026 station. Sh_1 shows three main peaks, (0.025, 0.028) m, (0.045, 0.050) m and 0.062 m respectively. The Sh_2 signal have same peaks, except the 0.062 m. Some vortices are also present near the limit of integration of the signals, respectively 114 cpm for Sh_1 and 102 cpm

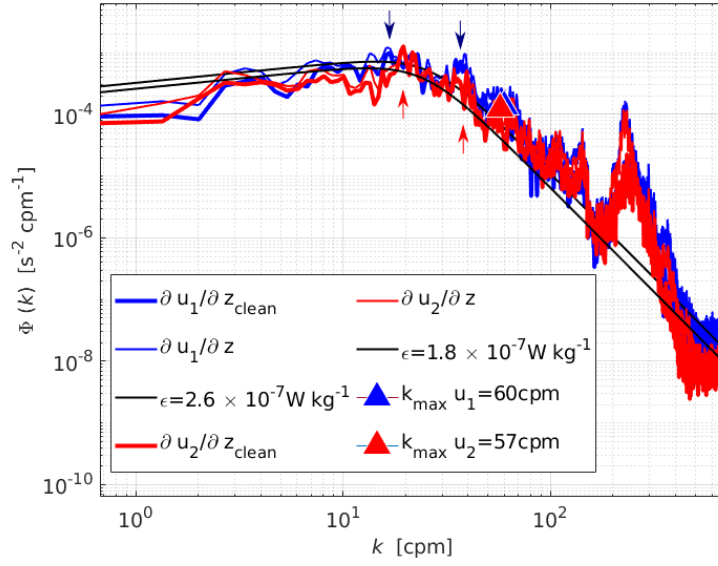
for Sh_2 , but are difficult to detect clearly on the graphic.

DAT_028 station is mainly characterized by a low limit of integration of both shear signals, *i.e.* 34 cpm for Sh_1 and 31 cpm for Sh_2 . At this station, Sh_1 and Sh_2 signals have different behaviour as indicated by the gap between the two Nasmyth models (the highest of the data set). Sh_1 has some significant vortices at (0.33, 0.05) m, 0.07 m, 0.10 m, 0.125 m and 0.285 m. Sh_2 highlights significant vortices only in the range (0.33, 0.05) m and at 0.285 m.

At DAT_029 station is characterised by both the various vortices recognized and the similarity of the two Nasmyth models on Sh_1 and Sh_2 . Both signals share same size of turbulent structures, except for 8.3 m vortices only presents on Sh_1 .

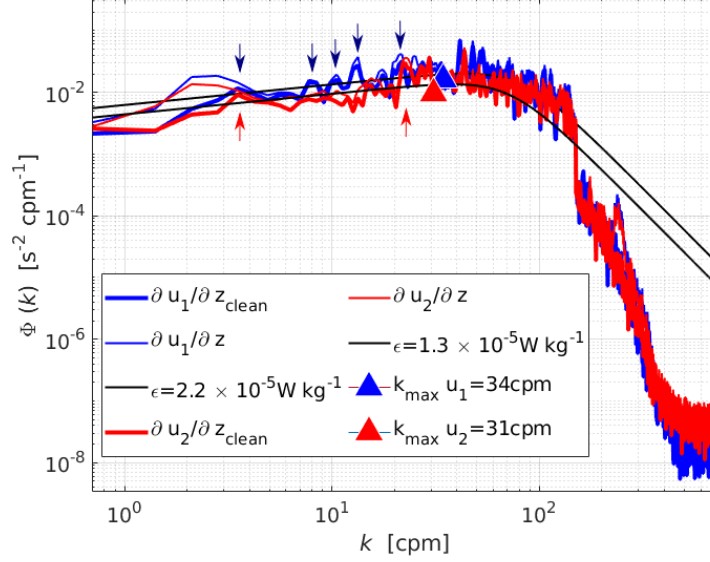


(a) Profile DAT_026

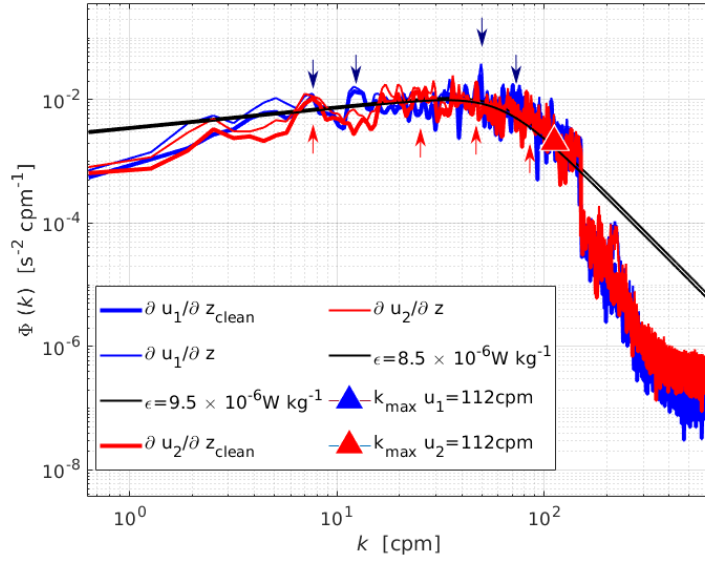


(b) Profile DAT_027

Figure 9: Wavenumber spectra of shear (blue and red) at DAT_026 and DAT_027 locations. The thin blue and red lines are the spectra without coherent-noise correction and the thick lines are the spectra after correction. The solid black lines are the empirical Nasmyth spectra for the dissipation rates indicated in the legend. Blue and red arrows highlight main k values recognized on respectively Sh_1 and Sh_2 clean signals. Both horizontal and vertical axis are in log scale.



(a) Profile DAT_028



(b) Profile DAT_029

Figure 10: Wavenumber spectra of shear (blue and red) at DAT_028 and DAT_029 locations. The thin blue and red lines are the spectra without coherent-noise correction and the thick lines are the spectra after correction. The solid black lines are the empirical Nasmyth spectra for the dissipation rates indicated in the legend. Blue and red arrows highlight main k values recognized on respectively Sh_1 and Sh_2 clean signals. Both horizontal and vertical axis are in log scale.

Table 1 summarize the information presented on figures 910 and , for each profile.

Profile	Energy	Sh ₁ (cm)	Sh ₂ (cm)	Anisotropy
DAT_026	Low	(3.50, 4.00), 5.80, 18.00	5.20, 13.30	Low $\varnothing_{SH1} \simeq \varnothing_{SH2}$
DAT_027	Medium	(2.50, 2.80), (4.50, 5.00), 6.25	(2.50, 2.80), (4.50, 5.00)	Low $\varnothing_{SH1} \simeq \varnothing_{SH2}$
DAT_028	Medium	(3.33, 5.00), 7.70, 10.00, 12.50, 28.50	(3.33, 5.00), 28.50	Medium $\varnothing_{SH1} \approx \varnothing_{SH2}$
DAT_029	High	(1.11, 1.60), 2.00, 8.33, 13.30	(1.50, 1.16), 2.00, (3.50, 4.00), 13.30	High $\varnothing_{SH1} < \varnothing_{SH2}$

Table 1: Characteristics summary of signals Sh₁ and Sh₂. Numbers indicate the size (cm) of recognized vortices.

For each station, wavelet analysis of Sh₁ and Sh₂ signals are showed on Fig.11 and Fig.12. In order to simplify interpretations, power wavelet coefficients with a p-value > 0.01 are removed from the figures. With such wavelet graphics, both vortex sizes and their location along the water column, can be defined. For each station, the colour scale is adapted as a function of each specific energetic range (from black for highest values to dark blue for the lowest ones), to better highlight wavelet coefficient variations inside each analysed signal. The abscissa represents the depth from -3.5 m to maximum depth reached by the VMP at the corresponding station and the y axis is the size of the vortices. The higher the coefficients, the more significant are the size.

Graphics on Fig.11 and Fig.12 were built so as to focus on main characteristics of the analysed signals. As an example of such graphics interpretation, Fig.11a shows Sh₁ power spectrum at station DAT_26. The first colour stain observed between depth from -3.5 to -5 m and for sizes from about 0.25 to 0.05 m, indicates that in the range depth (-3.5, -5) m, vortices in the range size (0.25, 0.05) m are present. The most significant sizes are ~ 0.15 m at ~ -4 m deep and ~ 0.10 m at ~ -5 m deep corresponding to two yellow colour spots. Other colour stains are indicators of existing vortices until the maximum depth.

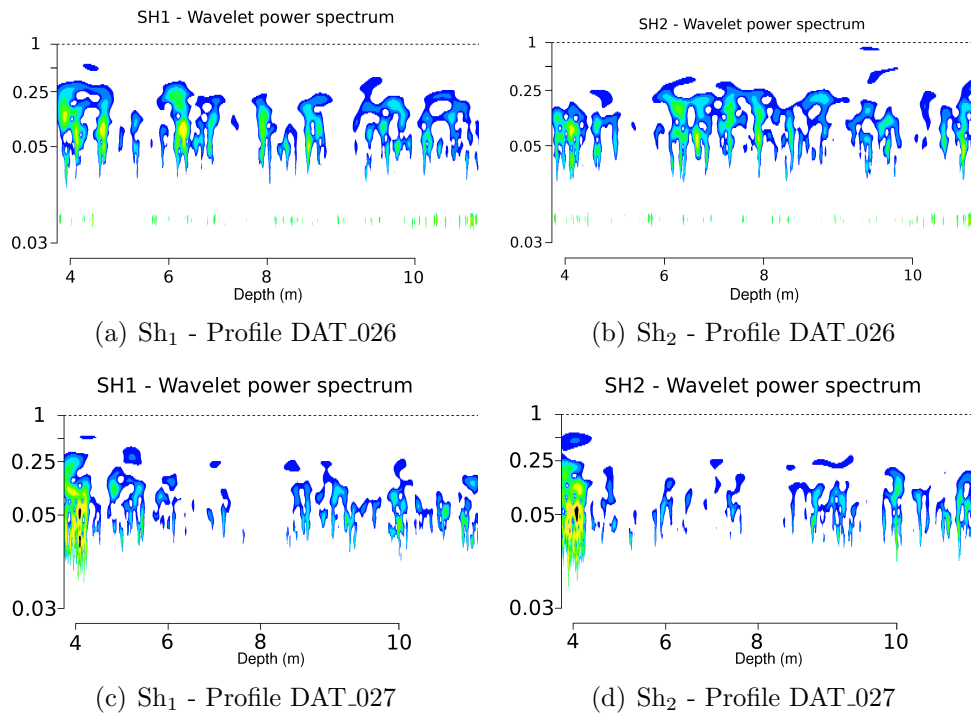


Figure 11: Power wavelet spectrum of Sh_1 and Sh_2 at stations DAT.26 and DAT.27. Power wavelet coefficients which are considered as non-significant (p -value > 0.01) are not showed. First column (a and c) contains power spectrum of Sh_1 and second column (b and d), those of Sh_2 , for each stations.

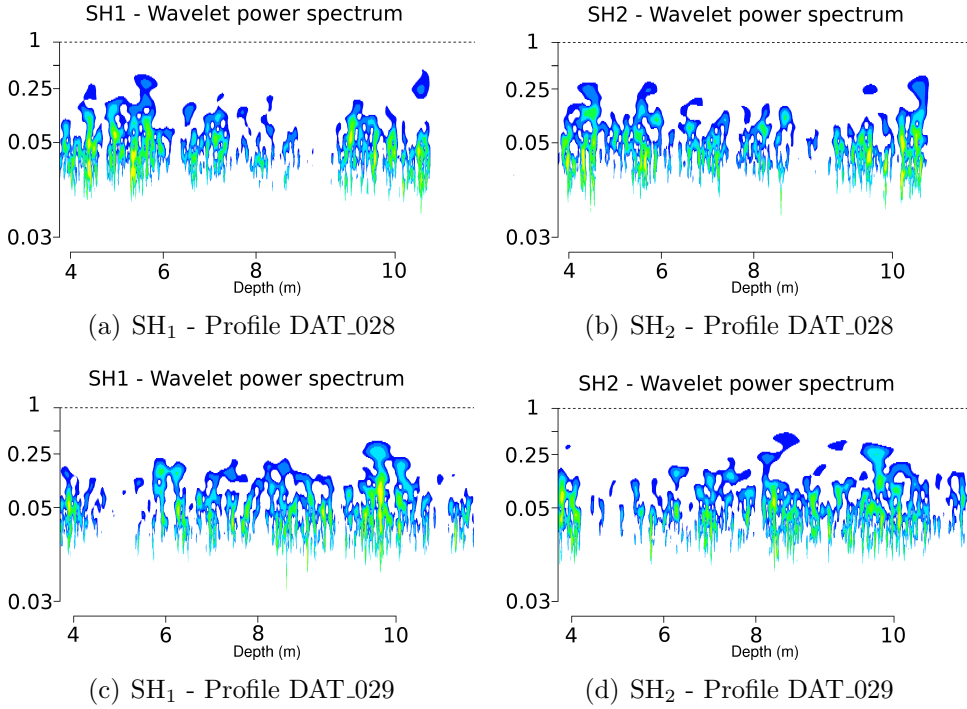


Figure 12: Power wavelet spectrum of Sh_1 and Sh_2 at stations DAT.28 and DAT.29. Power wavelet coefficients which are considered as non-significant (p -value > 0.01) are not showed. First column (a and c) contains power spectrum of Sh_1 and second column (b and d), those of Sh_2 , for each station.

Both Sh_1 and Sh_2 signals at DAT_026 station show wavelet significant coefficients characteristic of very small vortices, *i.e.* 0.05 m (Fig.11a-b). These structures represent the electronic noise of the VMP, thus the global energetic level of the signal at this station is very weak. A comparative study of Sh_1 and Sh_2 dataset highlight significant vortex (0.050, 0.250) m all along the water column.

Most of the turbulent energy at DAT_027 station is located between the surface to 4.5 m (Fig.11c-d). Below this depth, the wavelet analysis confirms the weak energy of the studied environment on two aspects, at the scale of the turbulent structures and at the scale station itself with a succession of depths without any turbulent structures.

DAT_028 station shows a higher energetic level both near the surface and at the end of the profile (Fig.12a-b). Between these two areas, the central part of the profile is characterized by both lower energetic and smaller sizes turbulent structures.

DAT_029 station, at the outlet of the studied area, highlights also two

turbulent domains (Fig.12c-d). The first is at the top of the water column, from surface to 4.5 m deep. The second turbulent domain is located between 6 m to the end of the profile. In this station, differences between the two shear signals are significant underlining the anisotropy of turbulent structures.

Analysis of VMP measurements allows to define an organization of the turbulence around a set of fish production structures compound composed of floating metallic frames on which nets are fixed.

The inlet current with a velocity of 0.45 m.s^{-1} flowing at 280° has a low level of turbulence along the water column (DAT_026 station). Some few isotropic vortices of small sizes ($< 0.2 \text{ m}$) are present along the depth which confer a high degree of homogeneity to this station. The outlet flow (DAT_029 station) has cross the set of fishnets along its longer side (180 m). At the rear of the cages, the energetic level is higher (x100) than at the inlet one. This is in particular the case from the sea surface to 4.5 m deep. The energetic vortices located in this area are due to the action of the flow on the floating metallic frame of the nets.

Near the bottom, the growing speed of the current and the wavy morphology of the sea-bed are responsible of highly energetic turbulent structures of bigger sizes ($> 0.25 \text{ m}$). Between these two areas, interactions cages-current generate turbulent vortex tied up to the wake effect as showed in Poizot et al. (2016). These two latter interactions, *i.e.* wake effect and bottom friction, create vortices of sizes ranging from 0.10 m to nearly 1 m. Wake effect vortices being clearly more anisotropic.

At the two stations DAT_027 and DAT_028 located sideways the fishnet structure, a high energetic level of turbulent vortices is present from the sea surface to 4.5 m deep. It corresponds to the same set of vortices highlighted at station DAT_029. Below this top area, the two stations highly differ in both size and intensity of the turbulent structures.

North the cages (DAT_027 station), most of the energetic turbulent structures are located in the upper part of the water column. Below, vortices, when present, are of small sizes and with low energy. Isotropic shape of both Sh_1 and Sh_2 signals can be due to the channelization of the current between the fishnets and central dike of the Cherbourg roadstead (Fig.1). Effects of the channelization prevailing on disturbances due to fishnets and could be the origin of small size vortices.

South, at DAT_028 station, the water column is more disturbed in relation with chains used to anchor the cages. The water flow action on the anchor chains and the mooring weights generate anisotropic vortices of variable sizes.

It appears that a weakly energetic current of 0.45 m.s^{-1} crossing a set of production nets of 180 m long, undergoes strong deformations. A first modification noticed on three sides of the net structure, is due to the metallic

floating part on which nets are anchored. At the rear of the cages, strong anisotropic eddies of various sizes confirm the presence of a water transport and associated particles (sediment, non-heated food, faeces, etc.) upward. This particular water circulation is reinforced by the flow acceleration under the cages and the associated eddies, produced by the growing bottom critical constraint. Environment of the cages has also to be taken into account. Here, the presence of a dike channelize the current flow making it more homogeneous, elsewhere, anchor chains disturb more or less locally the flow.

5. CONCLUSION

Analysis of VMP measurements performed around fishnet structures of on the salmon farm located in the Cherbourg roadstead, allow to give precise information of the turbulent characteristics of the water column in the near vicinity of the nets. This information is important for industrial and environmental interests.

Sizes of vortices, their isotropy/anisotropy, their intensity and also their localization along the water depth, have been quantify in an area under medium to high tide currents (up to 0.5 m.s^{-1}). The wavelet analysis conducted after the classical Fourier approach, demonstrated that the turbulence is not evenly distributed along the water column. Such information is for the first time highlighted here around fishnet production structures.

To help fish farmers to a better manage their production, complementary knowledge of turbulence characteristics must be conduct. The constant progress of technologies allows now to consider new monitoring approaches. With the growing measurement rate of ADCPs, turbulent structures up to 3-4 cm can be detected. New shape of VMPs allows simpler and safer deployments. The mix of both instruments family could gain access to more precise time and space understanding of the turbulence behaviour on the field.

Numerical simulations aiming to model currents/fishnet interactions under high Reynolds number conditions will also gain of such works. For example, it could help to set more accurately the turbulent model characteristics.

ACKNOWLEDGEMENTS

Funding was provided by the Normandy Regional Council, the Syndicat Mixte du Cotentin and the Conseil Départemental de la Manche. We thank AMP/GMG society and Construction Mécanique de Normandie (CMN) for their technical help and nautical support during the surveys. The authors would also like to thank anonymous reviewers for their constructive comments on the original manuscript.

References

- Bi, C.W., Zhao, Y.P., Dong, G.H., Zheng, Y.N., Gui, F.K., 2014. A numerical analysis on the hydrodynamic characteristics of net cages using coupled fluid-structure interaction model. *Aquacultural Engineering* 59, 1–12. URL: <http://www.sciencedirect.com/science/article/pii/S014486091400003X>, doi:10.1016/j.aquaeng.2014.01.002.
- Chamberlain, J., Stucchi, D., 2007. Simulating the effects of parameter uncertainty on waste model predictions of marine finfish aquaculture. *Aquaculture* 272, 296–311. URL: <http://www.sciencedirect.com/science/article/pii/S0044848607008988>, doi:10.1016/j.aquaculture.2007.08.051. number: 1.
- Chamberlain, J., Weise, A., Grant, J., Dowd, M., 2006. Modelling the effects of biodeposition from shellfish farms on the near field benthic environment. *dfo can. sci. advis. sec. res. doc.* 2006/03 ed. p. 50.
- Cornejo, P., Sepúlveda, H.H., Gutiérrez, M.H., Olivares, G., 2014. Numerical studies on the hydrodynamic effects of a salmon farm in an idealized environment. *Aquaculture* 430, 195–206. URL: <http://www.sciencedirect.com/science/article/pii/S0044848614001811>, doi:10.1016/j.aquaculture.2014.04.015.
- Cromey, C.J., Nickell, T.D., Black, K.D., 2002. DEPOMOD—modelling the deposition and biological effects of waste solids from marine cage farms. *Aquaculture* 214, 211–239. URL: <http://www.sciencedirect.com/science/article/pii/S004484860200368X>, doi:10.1016/S0044-8486(02)00368-X. number: 1.
- del Alamo, J., Jimenez, J., 2009. Estimation of turbulent convection velocities and corrections to Taylor’s approximation. *J. Fluid Mech.* 640, 5–26.
- Duarte, C.M., Holmer, M., Olsen, Y., Soto, D., MarbÃ , N., Guiu, J., Black, K., Karakassis, I., 2009. Will the Oceans Help Feed Humanity? *BioScience* 59, 967–976. URL: <https://academic.oup.com/bioscience/article/59/11/967/251334>, doi:10.1525/bio.2009.59.11.8. number: 11 Publisher: Oxford Academic.
- Food, Organization, A., 2020. The State of World Fisheries and Aquaculture 2020. FAO. URL: <http://www.fao.org/documents/card/en/c/ca9229en>, doi:10.4060/ca9229en.

- Gansel, L.C., Oppedal, F., Birkevold, J., Tuene, S.A., 2018. Drag forces and deformation of aquaculture cages-Full-scale towing tests in the field. *Aquacultural Engineering* 81, 46–56. URL: <http://www.sciencedirect.com/science/article/pii/S0144860917302170>, doi:10.1016/j.aquaeng.2018.02.001.
- Gjø sund, S.H., Enerhaug, B., 2010. Flow through nets and trawls of low porosity. *Ocean Engineering* 37, 345–354. URL: <http://www.sciencedirect.com/science/article/pii/S0029801810000119>, doi:10.1016/j.oceaneng.2010.01.003. number: 4.
- Gorle, J.M.R., Terjesen, B.F., Summerfelt, S.T., 2019. Hydrodynamics of Atlantic salmon culture tank: Effect of inlet nozzle angle on the velocity field. *Computers and Electronics in Agriculture* 158, 79–91. URL: <http://www.sciencedirect.com/science/article/pii/S0168169918307105>, doi:10.1016/j.compag.2019.01.046.
- Gowen, R., Bradbury, N., Brown, J., 1989. The use of simple models in assessing two interactions between fish farming and the marine environment. n. de paux, e. jaspers, n. wilkins (eds.) ed. pp. 1071–1080.
- Guerra, M., Thomson, J., 2017. Turbulence Measurements from Five-Beam Acoustic Doppler Current Profilers. *Journal of Atmospheric and Oceanic Technology* 34, 1267–1284. URL: <http://journals.ametsoc.org/doi/full/10.1175/JTECH-D-16-0148.1>, doi:10.1175/JTECH-D-16-0148.1.
- Holmer, M., 2010. Environmental issues of fish farming in offshore waters: perspectives, concerns and research needs. *Aquacult. Environ. Interact.* , 57–70.
- Johansson, D., Laursen, F., Fernö, A., Fosseidengen, J.E., Klebert, P., Stien, L.H., Vågseth, T., Oppedal, F., 2014. The Interaction between Water Currents and Salmon Swimming Behaviour in Sea Cages. *PLOS ONE* 9, e97635. URL: <https://journals.plos.org/plosone/article?id=10.1371/journal.pone.0097635>, doi:10.1371/journal.pone.0097635. number: 5 Publisher: Public Library of Science.
- Klebert, P., Patursson, O., Endresen, P.C., Rundtop, P., Birkevold, J., Rasmussen, H.W., 2015. Three-dimensional deformation of a large circular flexible sea cage in high currents: Field experiment and modeling. *Ocean Engineering* 104, 511–520. URL:

- <http://www.sciencedirect.com/science/article/pii/S0029801815001262>,
doi:10.1016/j.oceaneng.2015.04.045.
- Klebert, P., Su, B., 2020. Turbulence and flow field alterations inside a fish sea cage and its wake. *Applied Ocean Research* 98, 102113. URL: <http://www.sciencedirect.com/science/article/pii/S0141118719306716>, doi:10.1016/j.apor.2020.102113.
- Lader, P., Dempster, T., Fredheim, A., Jensen, C., 2008. Current induced net deformations in full-scale sea-cages for Atlantic salmon (*Salmo salar*). *Aquacultural Engineering* 38, 52–65. URL: <http://www.sciencedirect.com/science/article/pii/S0144860907000957>, doi:10.1016/j.aquaeng.2007.11.001. number: 1.
- Lu, Y., Lueck, R., 1999. Using a Broadband ADCP in a Tidal Channel. Part II: Turbulence. *Journal of Atmospheric and Oceanic Technology* 16, 1568–1579. doi:10.1175/1520-0426(1999)016.
- Lueck, R., 2015. Calculating the rate of dissipation of turbulent kinetic energy. techreport TN-028. RSI. URL: <http://rocklandscientific.com/?wpdmdl51034>.
- Lueck, R., Wolk, F., Black, K., 2013. Measuring tidal channel turbulence with a vertical microstructure profiler (VMP). Technical Report TN-026. RSI. URL: <http://www.rocklandscientific.com/Support/TechnicalNotes/tabid/68/Default.aspx>.
- Lueck, R.G., 2013. Calculating the rate of dissipation of turbulent kinetic energy. Technical Report TN-028. Rockland Scientific International. URL: <http://rocklandscientific.com/?wpdmdl51034>.
- Macoun, P., Lueck, R., 2004. Modeling the spatial response of the airfoil shear probe using different sized probes. *Journal of Atmospheric and Oceanic Technology* 21, 284–297. doi:10.1175/1520-0426(2004)02.
- Mallat, S., 1989. A theory for multiresolution signal decomposition: the wavelet representation. *IEEE Trans. Pattern Anal. Mach. Intell.* 11, 674–693.
- Masaló, I., Guadayol, O., Peters, F., Oca, J., 2008. Analysis of sedimentation and resuspension processes of aquaculture biosolids using an oscillating grid. *Aquacultural Engineering* 38, 135–144. URL:

- <http://www.sciencedirect.com/science/article/pii/S014486090800006X>, doi:10.1016/j.aquaeng.2008.01.004. number: 2.
- Massel, S., 2001. Wavelet analysis for processing of ocean surface wave records. *Ocean Engineering* 28, 957 – 987. URL: <http://www.sciencedirect.com/science/article/pii/S0029801800000445>, doi:[https://doi.org/10.1016/S0029-8018\(00\)00044-5](https://doi.org/10.1016/S0029-8018(00)00044-5).
- McMillan, J.M., Hay, A.E., Lueck, R.G., Wolk, F., 2015. An assessment of the dissipation rates at a tidal energy site using a vmp and an adcp, in: *European Wave and Tidal Energy Conference 2015*, Nantes, p. 8.
- Moin, P., 2009. Revisiting Taylor’s hypothesis. *Journal of Fluid Mechanics* 640, 1–4. doi:10.1017/s0022112009992126.
- Nasmyth, P.V., 1970. Ocean turbulence. Ph.D. thesis. URL: <http://hdl.handle.net/2429/34947>, doi:10.14288/1.0302459.
- Oakey, N., 1982. Determination of the rate of dissipation of turbulent energy from simultaneous temperature and velocity shear microstructure measurements. *Journal of Physical Oceanography* 12, 256–271.
- Panchang, V., Cheng, G., Newell, C., 1997. Modelling hydrodynamics and aquaculture waste transport in coastal maine. *Estuaries* , 14–41.
- Patursson, O., 2008. Flow through and around fish farming nets.
- Patursson, O., Swift, M.R., Tsukrov, I., Simonsen, K., Baldwin, K., Fredriksson, D.W., Celikkol, B., 2010. Development of a porous media model with application to flow through and around a net panel. *Ocean Engineering* 37, 314–324. URL: <http://www.sciencedirect.com/science/article/pii/S0029801809002406>, doi:10.1016/j.oceaneng.2009.10.001. number: 2.
- Poizot, E., Verjus, R., N’Guyen, H., Angilella, J., Mear, Y., 2016. Self-contamination of aquaculture cages in shallow water. *Environmental Fluid Mechanics* 16, 793–805. doi:10.1007/s10652-016-9450-7.
- R Core Team, 2016. R: A Language and Environment for Statistical Computing. R Foundation for Statistical Computing. Vienna, Austria. URL: <https://www.R-project.org/>.
- Roesch, A., Schmidbauer, H., 2014. Wavelet-Comp: Computational Wavelet Analysis. URL: http://www.hs-stat.com/projects/WaveletComp/WaveletComp_guided_tour.pdf.

- Skogen, M.D., Eknes, M., Asplin, L.C., Sandvik, A.D., 2009. Modelling the environmental effects of fish farming in a Norwegian fjord. *Aquaculture* 298, 70–75. URL: <http://www.sciencedirect.com/science/article/pii/S004484860900845X>, doi:10.1016/j.aquaculture.2009.10.018. number: 1.
- Stacey, M., Monismith, S., Burau, J., 1999. Measurements of Reynolds stress profiles in unstratified tidal flow. *Journal of Geophysical Research: Oceans* 104, 10933–10949. URL: <http://onlinelibrary.wiley.com/doi/10.1029/1998JC900095/abstract>, doi:10.1029/1998JC900095.
- Taylor, G.I., 1938. The spectrum of turbulence. *Proc. R. Soc. Lond.* 164, 476–490.
- Thetmeyer, H., Waller, U., Black, K.D., Inselmann, S., Rosenthal, H., 1999. Growth of European sea bass (*Dicentrarchus labrax* L.) under hypoxic and oscillating oxygen conditions. *Aquaculture* 174, 355–367. URL: <http://www.sciencedirect.com/science/article/pii/S0044848699000289>, doi:10.1016/S0044-8486(99)00028-9. number: 3.
- Torrence, C., Compo, G., 1998. A practical guide to wavelet analysis. *Bull. Am. Meteorol. Soc.* 79, 61–78.
- Tseng, Y., Shen, M., Jan, S., Dietrich, D., Chiang, C., 2012. Validation of the kuroshio current system in the dual-domain pacific ocean model framework. *Prog. Oceanogr.* 105, 102–124.
- Winthereig-Rasmussen, H., Simonsen, K., Patursson, O., 2016. Flow through fish farming sea cages: Comparing computational fluid dynamics simulations with scaled and full-scale experimental data. *Ocean Engineering* 124, 21 – 31. URL: <http://www.sciencedirect.com/science/article/pii/S0029801816302761>, doi:<https://doi.org/10.1016/j.oceaneng.2016.07.027>.
- Xu, J., Shen, H., Wang, H., 2015. An industry-scale modeling for the turbulence agglomeration of fine particles. *Advances in Mechanical Engineering* URL: <https://journals.sagepub.com/doi/10.1177/1687814015617670>, doi:10.1177/1687814015617670. publisher: SAGE PublicationsSage UK: London, England.
- Zhao, Y.P., Bi, C.W., Dong, G.H., Gui, F.K., Cui, Y., Xu, T.J., 2013. Numerical simulation of the flow field inside and

around gravity cages. *Aquacultural Engineering* 52, 1–13. URL:
<http://www.sciencedirect.com/science/article/pii/S0144860912000593>,
[doi:10.1016/j.aquaeng.2012.06.001](https://doi.org/10.1016/j.aquaeng.2012.06.001).

Declaration of interests

The authors declare that they have no known competing financial interests or personal relationships that could have appeared to influence the work reported in this paper.

The authors declare the following financial interests/personal relationships which may be considered as potential competing interests:

Emmanuel Poizot : Writing - Review & Editing, Formal analysis, Methodology, Conceptualization

Yann Méar : Writing - Review & Editing, Validation

Sylvain Guillou : Writing - Review & Editing, Funding acquisition

Eric Bibeau : Resources, Writing - Review & Editing, Funding acquisition